Dissecting Superradiant Phase Transition in the Quantum Rabi Model

Yun-Tong Yang(杨贇彤)[1,2] and Hong-Gang Luo(罗洪刚)[1,2*]

[1]*School of Physical Science and Technology, Lanzhou University, Lanzhou 730000, China*
[2]*Lanzhou Center for Theoretical Physics & Key Laboratory of Theoretical Physics of Gansu Province, Lanzhou University, Lanzhou 730000, China*

Phase transitions are both thermodynamically and quantum-mechanically ubiquitous in nature and laboratories, and their understanding remains one of the most active issues in modern physics and related disciplines. The Landau theory provides a general framework to describe *phenomenologically* phase transitions by introducing order parameters and associated symmetry breaking. This theory is also taken as a starting point to explore critical phenomena in connection with phase transitions in the renormalization group, which provides a complete theoretical description of behaviors close to critical points. In this context, the microscopic mechanism of phase transitions remains unclear. In this study, we explore the microscopic mechanism of the superradiant phase transition in the quantum Rabi model (QRM). First, we perform a diagonalization operation in an operator space to obtain three fundamental patterns, denoted as λ_1, λ_2, and λ_3, involved in the QRM. Then, we explicitly analyze the energy evolutions of these patterns with increasing coupling strength. The observed characteristic behaviors reveal the microscopic mechanism of the superradiant phase transition as a consequence of competition between patterns due to different phase relations. In other words, with increasing coupling strength, the pattern λ_1 drives the phase transition, the pattern λ_2 exhibits a similar response speed but less energy compensation than the pattern λ_1, and the pattern λ_3 exhibits a slow response speed but plays a key role in the balance between it and the pattern λ_1, which stabilizes the new phase. This type of dissecting mechanism explains why and how the superradiant phase transition occurs in the QRM and paves the way for exploring the microscopic mechanism of phase transitions that occur frequently in nature.

Introduction. The discovery of critical phenomena can be traced back to 1822 based on de la Tour's observations of supercritical liquids,[1] which were further refined by Andrews in 1869,[2] who defined the concept of critical points. In 1873, van der Waals proposed an equation of state, namely, the famous van der Waals equation, to theoretically explain the continuity of the gaseous and liquid states of matter.[3,4] Furthermore, Pierre Curie found in 1895 that ferromagnetic materials tend to lose their permanent magnetism once the temperature increases up to a certain value, known as the Curie temperature or the Curie point. In 1907, Weiss explained this phenomenon using his molecular mean-field theory.[5] In addition, in the 1930s, Bragg and Williams formulated the order-disorder transition in a binary alloy system.[6,7] Finally, in 1937, Landau presented a general and unified framework to treat *phenomenologically* these phase transitions by introducing the concept of order parameter, which is associated with certain broken symmetry.[8,9] This forms the foundation of modern phase transition theory and of analyzing critical behaviors.[10,11]

Although the concept of order parameter is still *phenomenological* in nature underlying mean-field treatment, the scaling analysis and renormalization group method developed in the 1960–1970s further proposes the concept of the universality class of phase transitions characterized by various critical exponents.[12,13] Despite intensive and extensive studies of the details of various phase transitions in the past decades, in particular the formulation of the renormalization group, it was clearly pointed out in the press release for the Nobel Prize that "*Wilson's theory for critical phenomena gave a complete theoretical description of the behaviour close to the critical point and gave also methods to calculate numerically the crucial quantities.*"[14] Based on the facts of the nature of phenomenology of the Landau's theory and the nature of descriptiveness of the Wilson's theory, the microscopic mechanism of phase transitions remains unexplored to a large extent.[15] Instead, the reason of phase transitions is usually attributed to thermodynamical (at finite temperature) or quantum mechanical (at zero temperature) *fluctuations* and the *competitions* between various possible orders during thermodynamical[10] or quantum phase transitions.[11] The causes, mechanisms, and occurrences of phase transitions remain unclear.

In this study, we explore this issue by taking the superradiant phase transition in the quantum Rabi model (QRM)[16–20] as an example. Early analysis of the ground state in the QRM[21,22] showed that the ground state exhibits a squeezing phenomenon in the strong, ultra-strong,

---

and deep-strong coupling regimes [23–28], a precursor of the distinguished physics of superradiance, which has been further confirmed theoretically. [29–41] Recently, this phase transition was observed in a single trapped ion [42,43] and simulated experimentally in a platform of nuclear magnetic resonance. [44] In Ref. [40], the present authors pointed out that the superradiant phase transition occurs due to the appearance of the induced double-well potential when the coupling strength increases across its critical point. Here, we further explore why and how the phase transition occurs.

Methodologically, in contrast to Ref. [40], we first perform a diagonalization in an operator space (see below) to obtain three fundamental patterns, denoted as λ_1, λ_2, and λ_3, which are exact in the sense that the Hamiltonian matrix can be exactly reproduced for a given Fock basis. To further confirm the validity of the pattern picture, we compare the energy levels, the mean photon numbers, and spin-flip for the first four states with those obtained by numerical exact diagonalization (ED). Then, we analyze the ground-state superradiant phase transition by determining the energy levels of the ground and first excited states, which almost degenerate in the superradiant phase. The patterns λ_1, λ_2, and λ_3 play different roles in the superradiant phase transition due to the competition between them: with increasing coupling strength, the pattern λ_1 drives the occurrence of the superradiant phase transition by rapidly lowering the energy of the system as the coupling strength approaches its critical point; the pattern λ_2 exhibits a similar response speed but has a less contribution to the ground state; the pattern λ_3 exhibits a slow response but has an important contribution to the ground state to balance the pattern λ_1. Thus, the system is stable in the new phase. The different roles of the three patterns reveal why and how the superradiant phase transition occurs in the QRM, supporting our approach to microscopically examine the superradiant phase transition. Both methodologically and physically, our results pave the way for exploring phase transitions in other systems.

Model and Method. The standard Hamiltonian of the QRM reads

$$\hat{H} = \hbar\omega\left(\hat{a}^\dagger\hat{a} + \frac{\Delta}{2}\hat{\sigma}_x + g(\hat{a} + \hat{a}^\dagger)\hat{\sigma}_z\right), \qquad (1)$$

where $\hat{a}^\dagger(\hat{a})$ is the creation (annihilation) operator of the single-photon mode and $\hat{\sigma}_{x(z)}$ is Pauli matrix denoting the two-level atom. For convenience, we rescale the Hamiltonian by the mode frequency $\hbar\omega$; thus, the energy interval Δ and the coupling strength g used in the following are dimensionless, and the units of energy $\hbar\omega$ are omitted for simplicity. By using the relation $\hat{\sigma}_y\hat{\sigma}_z = i\hat{\sigma}_x$, Eq. (1) can be reformulated as follows:

$$\hat{H} = \begin{pmatrix} -i\hat{\sigma}_y & \hat{\sigma}_z & \hat{a}^\dagger \end{pmatrix} \begin{pmatrix} 0 & \frac{\Delta}{4} & 0 \\ \frac{\Delta}{4} & 0 & g \\ 0 & g & 1 \end{pmatrix} \begin{pmatrix} i\hat{\sigma}_y \\ \hat{\sigma}_z \\ \hat{a} \end{pmatrix} \qquad (2)$$

$$= \sum_{n=1}^{3} \lambda_n \hat{A}_n^\dagger \hat{A}_n, \qquad (3)$$

$$\hat{A}_n = u_{n,1}(i\hat{\sigma}_y) + u_{n,2}\hat{\sigma}_z + u_{n,3}\hat{a}, \qquad (4)$$

where $\{\lambda_n, u_n\}(n = 1, 2, 3)$ are the eigenvalues and eigenvectors of the matrix in Eq. (2), forming three basic patterns denoted as the eigenenergies λ_n and corresponding eigenvectors [Figs. 1(a1)–1(a3)]. Before discussing the explicit physics of the phase transition, it is necessary to verify the validity of the obtained pattern picture.

Patterns and Solution. Equation (3) can be solved by inserting into the complete basis $|\sigma_z, m\rangle$, where $\hat{\sigma}_z|\sigma_z\rangle = \pm(\uparrow, \downarrow)|\sigma_z\rangle$ denoting the spin eigenstate along the z-direction and $\hat{a}^\dagger\hat{a}|m\rangle = m|m\rangle(m = 0, 1, \ldots, N)$ denoting the truncated Fock basis with the photon number m. First, the matrix $[\hat{A}_n]_{\sigma_z, m; \sigma_z', m'} = \langle\sigma_z, m|\hat{A}_n|m', \sigma_z'\rangle$ is obtained; then, Eq. (3) can be solved by diagonalizing the matrix obtained by

$$\langle\sigma_z, m|\hat{H}|m', \sigma_z'\rangle = \sum_{n=1}^{3} \lambda_n \langle\sigma_z, m|\hat{A}_n^\dagger\hat{A}_n|m', \sigma_z'\rangle$$

$$= \sum_{n=1}^{3} \lambda_n \sum_{\sigma_z'', m''} [\hat{A}_n^\dagger]_{m, \sigma_z; m'', \sigma_z''}[\hat{A}_n]_{m'', \sigma_z''; m', \sigma_z'}. \qquad (5)$$

After obtaining the eigenstate wavefunctions Ψ_i ($i = 0, 1, \ldots$, corresponding to the ground state, the first excited state, and so on, respectively), the wavefunctions are projected onto different patterns to calculate the contributions of the different patterns to the target physical quantities. For example, the energy contributions of the three patterns to the eigenstate Ψ_i can be calculated as follows:

$$E_{\lambda_n} = \langle\Psi_i|\lambda_n\hat{A}_n^\dagger\hat{A}_n|\Psi_i\rangle, (n = 1, 2, 3). \qquad (6)$$

From the calculation of $\langle\Psi_i|\hat{A}_n^\dagger\hat{A}_n|\Psi_i\rangle$, the related physical observables can be extracted, such as $\langle\Psi_i|\hat{a}^\dagger\hat{a}|\Psi_i\rangle_{\lambda_n} = u_{n,3}^2\langle\Psi_i|\hat{a}^\dagger\hat{a}|\Psi_i\rangle$ and $\langle\Psi_i|\hat{\sigma}_x|\Psi_i\rangle_{\lambda_n} = u_{n,1}u_{n,2}\langle\Psi_i|\hat{\sigma}_x|\Psi_i\rangle$, which are easily calculated once Ψ_i are obtained by diagonalizing the Hamiltonian matrix Eq. (5). Before discussing the physics of the phase transition, we first check the validity of the above formalism.

Figures 1(b1)–1(b3) present the first four energy levels for the three patterns by taking a truncated Fock basis with $N = 200$. A dramatic energy change occurs in all three patterns around the coupling strength $g/g_c \sim 1.0$, which indicates the occurrence of a superradiant phase transition in the system, a well-known result in the literature. [30,32] The validity of our formalism is confirmed by comparing the summation (solid lines) of respective physical quantities for all three patterns, for example, the energies shown in Figs. 1(b1)–1(b3), to those obtained directly by ED (symbols). The results are the same, as shown in Fig. 1(c) for the energy levels, Fig. 1(d) for the photon number $\langle\hat{a}^\dagger\hat{a}\rangle$, and Fig. 1(e) for the spin-flip $\langle\hat{\sigma}_x\rangle$ (for the latter two quantities, the respective pattern components have not been shown here). This is not surprising because no additional approximation has been introduced in the pattern formalism compared with ED formalism. Thus, the above formalism provides an alternative way to dissect the Hamiltonian of the QRM into fundamental patterns, providing a novel perspective to analyze the physics involved in the QRM, for example, the superradiant phase transition we focus on here.
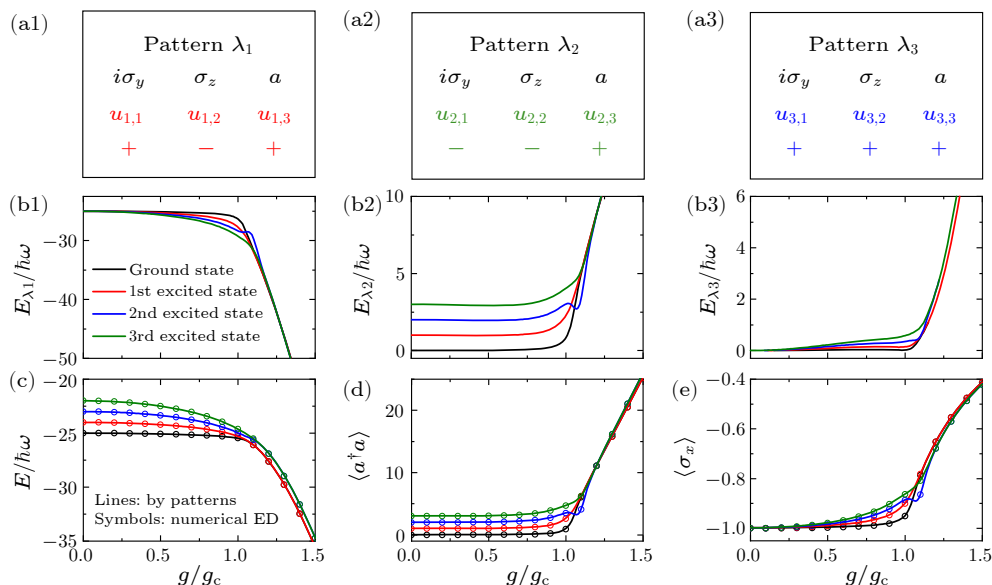
Fig. 1. Marks of obtained patterns and comparisons of physical quantities with results obtained by ED. (a1)–(a3) Patterns marked by λ_1, λ_2, and λ_3 and corresponding eigenvectors with relative phase denoted by $\pm$. Note that there is a total free-phase factor $e^{i\pi}$, which is omitted here for simplicity. (b1)–(b3) First four pattern energy levels as functions of coupling strength rescaled by $g_c = \sqrt{1 + \sqrt{1 + \frac{\Delta^2}{16}}}$ [31] and $\Delta = 50$. (c) Summations of pattern energy levels (lines) and their comparison with the results obtained directly by ED (symbols). (d) Comparison of the summations of the patterns' photon number $\langle a^\dagger a \rangle_{\lambda_n} (n = 1, 2, 3)$ (not shown) to those obtained by ED (symbols). (e) Comparison of the summations of the $\langle \sigma^x \rangle_{\lambda_n}$ of patterns ($n = 1, 2, 3$) (not shown) to those obtained by ED (symbols). In the above comparisons, the first four energy levels are used.

Nature of Phase Transition. The QRM involves a superradiant phase transition as the coupling strength $g/g_c \sim 1.0$, where the energy levels, mean photon numbers, and spin-flip change dramatically [Figs. 1(c)–1(e)]. We perform detailed and deeper analysis of why and how the phase transition occurs by carefully checking the different contributions of the different patterns to the ground and first excited states, from which the competition between the different patterns can be observed. In Fig. 2(a1), in the weak coupling regime, the ground state of the system is completely dominated by the pattern λ_1 (thin red line), whereas the other patterns do not contribute to the ground state. This regime is a well-known normal phase in which the photon number is zero. With increasing coupling strength, the system enters the superradiant phase, and the behaviors of different patterns can be evaluated. First, the pattern λ_1 exhibits an obvious downturn and then descends continually. The pattern λ_2 exhibits a similarly rapid response to the change in the form of compensation. This is physically reasonable because the system exhibits a trend to remain in its previous state. However, the contribution from the pattern λ_2 is not sufficient to compensate for the rapid increase in the contribution from the pattern λ_1; as a result, the pattern λ_3 begins to become a main contribution in balance to the pattern λ_1 [Fig. 2(a2)], and the second-order derivatives of the contributions of the patterns λ_1 and λ_3 exhibit similar changes but opposite trends with increasing coupling strength in the superradiant phase. The competition between the patterns λ_1 and $\lambda_{2,3}$ uncovers the microscopic mechanism of the superradiant phase transition: by increasing the cou-

pling strength, the photons are excited to decrease the energy of the system driven by the pattern λ_1. To balance the energy decrease caused by the pattern λ_1, the patterns $\lambda_{2,3}$ contribute positive energy, which stabilizes the system in the newly developed superradiant phase. The competition and balance relations reveal why and how the superradiant phase transition occurs in the QRM.

A similar behavior was observed in the first excited state [Figs. 2(b1) and 2(b2)]. In particular, the inset in
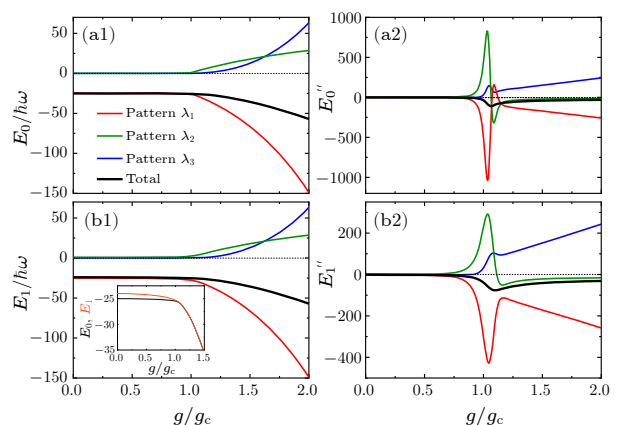

Fig. 2. (a1), (b1) Energy levels of ground and first excited states (heavy black solid lines) and corresponding pattern components (thin red, green, and blue solid lines) as functions of coupling strength. (a2), (b2) Second-order derivatives of the corresponding energy levels (heavy black solid lines) and their pattern components (thin red, green, and blue solid lines). The inset shows the energy levels of the ground and first excited states.

Fig. 2(b1) shows the close of the energy gap between the first excited state and the ground state, which is a typical behavior of the superradiant phase transition.
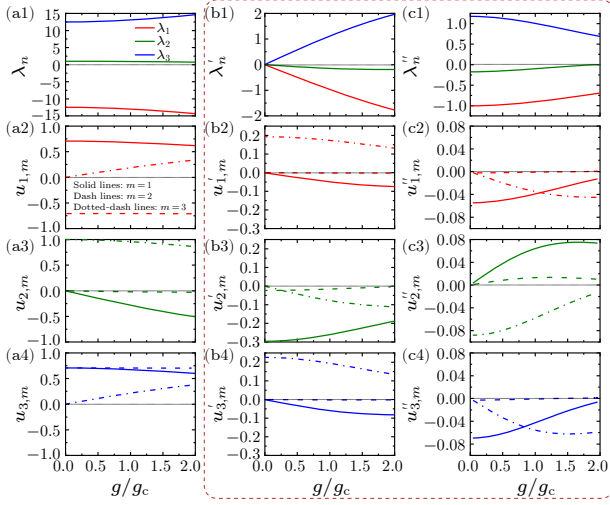

Fig. 3. Patterns marked by their eigenenergies and eigenfunctions as functions of coupling strength. The first column: (a1) the eigenenergy of the pattern $\lambda_n (n = 1, 2, 3)$; (a2) eigenfunctions $u_{1,m} (m = 1, 2, 3)$; (a3) eigenfunctions $u_{2,m}$; and (a4) eigenfunctions $u_{3,m}$. The second column: (b1)–(b4) first-order derivatives of the corresponding (a1)–(a4) with respect to the coupling strength. The third column: (c1)–(c4) the second-order derivatives of the corresponding (a1)–(a4) with respect to coupling strength. For each pattern, three components correspond to the operators $i\hat{\sigma}_y$ (solid lines), $\hat{\sigma}_z$ (dash lines), and $\hat{a}$ (dotted-dash lines).

After discussing the competition and balance relations between the different patterns during the phase transition, it is useful to further explore the properties of the patterns because the pattern picture is presented for the first time in the literature. Figure 3 shows the eigenenergies λ_n and corresponding eigenvectors $u_{n,i}(n, i = 1, 2, 3)$ of the patterns and their first- and second-order derivatives as functions of the coupling strength. A few properties are noted: (i) the signs or relative phases between the components in each pattern remain fixed [Figs. 1(a1)–1(a3)], which can be used to mark the patterns; (ii) in the patterns λ_1 and λ_3, the components $i\hat{\sigma}_y$ and $\hat{\sigma}_z$ representing the state of the two-level atom dominate over the component $\hat{a}$ representing the photon mode [Figs. 3(a2) and 3(a4)]; (iii) in the pattern λ_2, the photon mode is dominant and the weight of the first component $i\hat{\sigma}_y$ increases with increasing coupling strength, and that of the second component $\hat{\sigma}_z$ remains negligible in the entire coupling regime [Fig. 3(a3)]; (iv) the first- and second-order derivatives of the pattern eigenenergies and eigenvectors shown in Figs. 3(b1)–3(b4) and Figs. 3(c1)–3(c4), respectively, indicate that the patterns exhibit no singular behavior. These properties indicate that the patterns $\hat{A}_n$ are single-body operators from which no information about the phase transition can be obtained. In contrast, the competition and balance between the different patterns play key roles in the phase transition. This is the focus of this study: the microscopic mechanism of the phase transition.
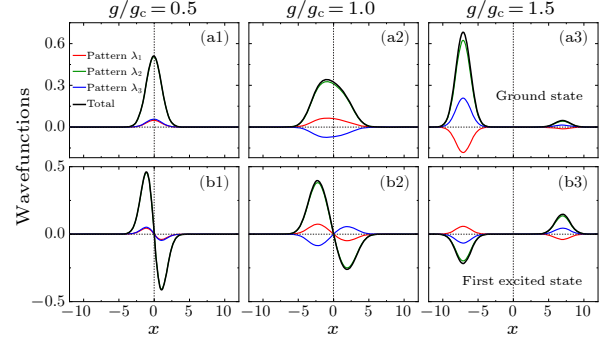

Fig. 4. Wavefunctions and their dissections given by $u_{n,3}|\Psi_i\rangle$ of the ground state (a1)–(a3) and first excited state (b1)–(b3) for three typical coupling strengths $g/g_c = 0.5$ (a1) and (b1); 1.0 (a2) and (b2); 1.5 (a3) and (b3), corresponding to the normal, critical, and superradiant phases, respectively, in the Fock basis. The heavy black solid lines denote the total wavefunctions, and the thin colored lines (red, green, and blue) correspond to the three components in the patterns λ_1, λ_2, and λ_3, respectively.
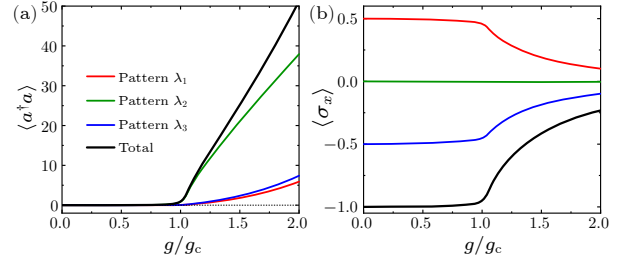

Fig. 5. Total photon number (a) and spin-flip (b), and the corresponding components in the patterns for the ground state as functions of coupling strength. The black solid lines denote the total, and the red, green, and blue thin solid lines denote the components in patterns λ_1, λ_2, and λ_3, respectively.

To evaluate the contributions of the patterns to the superradiant phase, the wavefunctions of the system consisting of the direct product of the two levels and the Fock basis of the photon mode were investigated. Here, we only present the up-spin branch. Figure 4 shows the results for the ground state (the first row) and first excited state (the second row). Figures 5(a) and 5(b) plot the physical observables $\langle\hat{a}^\dagger\hat{a}\rangle_{\lambda_n}$ and $\langle\hat{\sigma}_x\rangle_{\lambda_n}$, respectively. In all regimes, the pattern λ_2 accounts for almost all weight of the photon mode but makes a negligible contribution to the spin-flip [Fig. 5(b)]. In the superradiant phase, the contributions from all patterns are displaced from the zero point of the harmonic oscillator describing the photon mode, which is a typical feature of the superradiant phase. The contributions from the patterns λ_1 and λ_3 have an opposite phase, which indicates their competing relation. This is also obvious from the different phase relations shown in Figs. 1(a1) and 1(a3). With increasing coupling strength, the spin degree of freedom is strongly coupled to the photon mode; the superradiant photons dominate the system, and the influence of the spin degree of freedom is gradually suppressed, as shown in Fig. 5(b). These results provide insights into the physics of the strongly coupled regime of the QRM from the pattern picture, which deserves further exploration.

Summary and Outlook. In this study, we propose a scheme to analyze the physics of the superradiant phase transition from a microscopic viewpoint represented by a newly developed picture, namely, the pattern picture. This was obtained by diagonalizing the original Hamiltonian in the operator space $\{i\hat{\sigma}_y, \hat{\sigma}_z, \hat{a}\}$, which is different from typical methods in the literature. Using the pattern picture, we uncovered the microscopic mechanism of the superradiant phase transition in the QRM by dissecting the contributions of the obtained patterns to the ground and first excited states, thereby demonstrating the competition and balance relations between the patterns during the phase transition. Due to the fundamental role of the QRM in describing the interactions between light and matter, it is expected that the dissection of the obtained patterns can be further extended to more complex models, such as Dicke[45] and spin-boson models,[46] to understand additional intriguing physics involved in these models, such as the decoherence and dissipation mechanisms.

References

[1] Berche B, Henkel M, and Kenna R 2009 *Revista Brasileira de Ensino de Física* **31** 2602

[2] Rowlinson J S 2003 *Notes Rec. R. Soc. Lond.* **57** 143

[3] van der Waals J D 1873 *Over de continuiteit van den gas-en vloeistoftoestand* thesis (Univ. Leiden)

[4] ROWLINSON J S 1973 *Nature* **244** 414

[5] Weiss P 1907 *J. Phys. Theor. Appl.* **6** 661

[6] Bragg W L and Williams E J 1934 *Proceedings of the Royal Society of London. Series A, Containing Papers of a Mathematical and Physical Character* **145** 699

[7] Bragg W L and Williams E J 1935 *Proceedings of the Royal Society of London. Series A, Mathematical and Physical Sciences* **151** 540

[8] Landau L D 1937 *Phys. Z. Sowjet.* **11** 26

[9] Landau L D and Lifshitz E M 1980 *Course of Theoretical Physics Vol. 5 Statistical Physics Part I & II 3rd ed* (Elsevier Ltd., Amsterdam)

[10] Chaikin P M and Lubensky T C 2000 *Principles of condensed matter physics* (Cambridge University Press)

[11] Sachdev S 2011 *Quantum phase transitions* second ed. (Cambridge University Press)

[12] Wilson K G and Kogut J 1974 *Phys. Rep.* **12** 75

[13] Hahne F J W 1982 *In Critical Phenomena: Proceedings of the Summer School Held at the University of Stel-lenbosch* (Springer-Verlag 1983)

[14] See e.g., https://www.nobelprize.org/prizes/physics/1982/pressrelease/

[15] Kastner M 2008 *Rev. Mod. Phys.* **80** 167

[16] Rabi I I 1936 *Phys. Rev.* **49** 324

[17] Rabi I I 1937 *Phys. Rev.* **51** 652

[18] Braak D 2011 *Phys. Rev. Lett.* **107** 100401

[19] Chen Q H, Wang C, He S, Liu T, and Wang K L 2012 *Phys. Rev. A* **86** 023822

[20] Braak D, Chen Q H, Batchelor M T, and Solano E 2016 *J. Phys. A* **49** 300301

[21] Ashhab S and Nori F 2010 *Phys. Rev. A* **81** 042311

[22] Hwang M J and Choi M S 2010 *Phys. Rev. A* **82** 025802

[23] Wallraff A, Schuster D I, Blais A, Frunzio L, Huang R S, Majer J, Kumar S, Girvin S M, and Schoelkopf R J 2004 *Nature* **431** 162

[24] Niemczyk T, Deppe F, Huebl H, Menzel E P, Hocke F, Schwarz M J, Garcia-Ripoll J J, Zueco D, Hümmer T, Solano E, Marx A, and Gross R 2010 *Nature Physics* **6** 772

[25] Casanova J, Romero G, Lizuain I, García-Ripoll J J, and Solano E 2010 *Phys. Rev. Lett.* **105** 263603

[26] Yoshihara F, Fuse T, Ashhab S, Kakuyanagi K, Saito S, and Semba K 2017 *Nature Physics* **13** 44

[27] Yoshihara F, Fuse T, Ao Z, Ashhab S, Kakuyanagi K, Saito S, Aoki T, Koshino K, and Semba K 2018 *Phys. Rev. Lett.* **120** 183601

[28] Mueller N S, Okamura Y, Vieira B G M, Juergensen S, Lange H, Barros E B, Schulz F, and Reich S 2020 *Nature* **583** 780

[29] De Liberato S and Ciuti C 2013 *Phys. Rev. Lett.* **110** 133603

[30] Hwang M J, Puebla R, and Plenio M B 2015 *Phys. Rev. Lett.* **115** 180404

[31] Ying Z J, Liu M, Luo H G, Lin H Q, and You J Q 2015 *Phys. Rev. A* **92** 053823

[32] Liu M, Chesi S, Ying Z J, Chen X, Luo H G, and Lin H Q 2017 *Phys. Rev. Lett.* **119** 220601

[33] Wang Y, You W L, Liu M, Dong Y L, Luo H G, Romero G, and You J Q 2018 *New Journal of Physics* **20** 053061

[34] Peng J, Rico E, Zhong J X, Solano E, and Egusquiza I L 2019 *Phys. Rev. A* **100** 063820

[35] Zhu H J, Xu K, Zhang G F, and Liu W M 2020 *Phys. Rev. Lett.* **125** 050402

[36] Garbe L, Bina M, Keller A, Paris M G A, and Felicetti S 2020 *Phys. Rev. Lett.* **124** 120504

[37] Jiang X, Lu B, Han C, Fang R, Zhao M, Ma Z, Guo T, and Lee C 2021 *Phys. Rev. A* **104** 043307

[38] Zhuang W F, Geng B, Luo H G, Guo G C, and Gong M 2021 *Phys. Rev. A* **104** 053308

[39] Stránský P, Cejnar P, and Filip R 2021 *Phys. Rev. A* **104** 053722

[40] Yang Y T and Luo H G 2023 *Chin. Phys. Lett.* **40** 020502

[41] Duan L, Xie Y F, Braak D, and Chen Q H 2016 *J. Phys. A* **49** 464002

[42] Cai M L, Liu Z D, Zhao W D, Wu Y K, Mei Q X, Jiang Y, He L, Zhang X, Zhou Z C, and Duan L M 2021 *Nat. Commun.* **12** 1126

[43] Cai M L, Liu Z D, Jiang Y, Wu Y K, Mei Q X, Zhao W D, He L, Zhang X, Zhou Z C, and Duan L M 2022 *Chin. Phys. Lett.* **39** 020502

[44] Chen X, Wu Z, Jiang M, Lü X Y, Peng X, and Du J 2021 *Nat. Commun.* **12** 6281

[45] Dicke R H 1954 *Phys. Rev.* **93** 99

[46] Leggett A J, Chakravarty S, Dorsey A T, Fisher M P A, Garg A, and Zwerger W 1987 *Rev. Mod. Phys.* **59** 1